

2 **Origin of the magnetic field enhancement of the spin signal in metallic non-local spin**  
3 **transport devices**

4 A. J. Wright<sup>1</sup>, M. J. Erickson<sup>2</sup>, D. Bromley<sup>1</sup>, P. A. Crowell<sup>2</sup>, C. Leighton<sup>3</sup> and L. O'Brien<sup>1,\*</sup>

5 <sup>1</sup> Department of Physics, University of Liverpool, Liverpool, L69 7ZE, UK

6 <sup>2</sup> School of Physics and Astronomy, University of Minnesota, MN, 55455, USA

7 <sup>3</sup> Department of Chemical Engineering and Materials Science,

8 University of Minnesota, MN, 55455, USA

9  
10 The non-local spin valve (NLSV) enables unambiguous study of spin transport, owing to its  
11 ability to isolate pure spin currents. A key principle of NLSV operation is that the ‘spin signal’  
12 is invariant under application of in-plane magnetic fields (above the ferromagnetic contact  
13 saturation field). Yet, for certain ferromagnet/normal metal pairings in NLSVs, an unexpected  
14 field enhancement of the spin signal occurs, presenting a challenge that has, thus far, been  
15 difficult to resolve with existing models. By correlating the extracted spin transport parameters  
16 with material, temperature and field dependencies, in this work we identify field-quenching of  
17 magnetic impurity scattering as the origin of this effect, confirmed by excellent agreement  
18 between our results and field-dependent Kondo theory. In addition to addressing this long-  
19 standing mystery, our findings highlight a potential systematic underestimation of spin  
20 transport parameters. By identifying signature field and temperature dependencies, we provide  
21 here a relatively simple means to isolate and quantify this additional relaxation mechanism.

22 \*Corresponding author: lobrien@liverpool.ac.uk

## I. INTRODUCTION

1  
2 The controlled transport and manipulation of spins in metals offers the prospect of various  
3 technological advances in sensing, logic, and data storage. As an example, the problematic  
4 resistance scaling at low dimensions<sup>1-3</sup> of magnetic tunnel junctions in hard disk drive read  
5 head sensors provides a clear motivation to develop all-metal-based alternatives. Efforts to  
6 further understand the flow of spins between, and relaxation within, ferromagnetic (FM) and  
7 non-magnetically-ordered metals (NM)<sup>4-22</sup>, thus continue to gather pace. Despite this concerted  
8 effort, key fundamental questions remain open. Among these, the impact of specific scattering  
9 sources on spin relaxation in NMs is a recurring theme<sup>11,21,23-25</sup>, as are the origins of several  
10 field-dependent magnetoresistive effects.<sup>6,26-28</sup> Light metals, such as Cu and Al, offer an  
11 excellent testing ground to understand such issues. In essence, the low resistivity and spin-orbit  
12 coupling (SOC) in such metals result in relatively long spin lifetimes,  $\tau_s$ , where specific  
13 relaxation mechanisms can be intentionally introduced, e.g., through tuning disorder;<sup>29</sup> doping  
14 with high SOC<sup>30</sup> or magnetic impurities;<sup>13</sup> or manipulation of interfaces<sup>31</sup> and surfaces.<sup>8,22,23</sup>

15 The non-local spin valve (NLSV) geometry offers a particularly simple, versatile means to  
16 probe spin transport in light metals with long  $\tau_s$ .<sup>5</sup> Fig. 1(a) shows a scanning electron  
17 microscope (SEM) image of a typical nanoscopic metallic NLSV device. In the NLSV  
18 geometry, a NM channel is contacted by two FM nanowires,  $\text{FM}_{\text{inj}}$  and  $\text{FM}_{\text{det}}$ , separated by a  
19 distance,  $d$ . A charge current,  $I$ , flowing from  $I^+$  to  $I^-$  (see Fig. 1(a)) becomes spin-polarized  
20 in  $\text{FM}_{\text{inj}}$ , thus injecting spins into the NM, which subsequently diffuse along the NM channel  
21 in the form of a pure spin current. The resulting spin-accumulation reaching  $\text{FM}_{\text{det}}$  can be  
22 detected *via* the potential difference,  $V_{NL}$ , that develops between  $\text{FM}_{\text{det}}$  and the NM, i.e.,  
23 between  $V^+$  and  $V^-$ , which can then be normalized by  $I$  to give a non-local transimpedance,  
24  $R_{NL} = V_{NL}/I$ . Inevitably, in addition to the spin-accumulation signal, the measured  $R_{NL}$  also  
25 contains contributions from spurious effects, including finite current spreading<sup>32</sup> and

1 thermoelectric voltages.<sup>33–36</sup> To mitigate their impact on measurements, the standard approach  
 2 is to toggle the magnetization of the FM contacts, from parallel (P) to anti-parallel (AP), with  
 3 the difference between the two states,  $\Delta R_{NL} = R_{NL}^P - R_{NL}^{AP}$ , theoretically isolating only the ‘spin  
 4 signal’. Equivalently, one can explicitly calculate the background contribution from the  
 5 average of the two states, as  $R_b = (R_{NL}^P + R_{NL}^{AP})/2$ . The spin signal is then given by  $R_{spin} =$   
 6  $R_{NL}^P - R_b$ , as is the approach taken here. We note that these two approaches are mathematically  
 7 equivalent, save for a factor of 2, i.e.,  $\Delta R_{NL} = 2R_{spin}$ .

8 An example of the in-plane magnetic field,  $H||y$ , dependence of  $R_{NL}(H)$  is shown in Fig.  
 9 1(b) for a Cu/Fe NLSV with  $d = 750$  nm, over a moderate  $H$  range (up to 100 mT) and at a  
 10 measurement temperature,  $T = 5$  K. Both forward and reverse sweeps are shown, and  $R_{NL}^P$ ,  
 11  $R_{NL}^{AP}$  and  $R_b$  are clearly visible as the two FMs switch relative orientation. By measuring  $R_{spin}$   
 12 in devices with varying  $d$ , and fitting  $R_{spin}(d, T)$  using a suitable model,<sup>15,37</sup> key spin transport  
 13 parameters may be extracted for the NM channel under investigation, particularly the  
 14 characteristic NM spin diffusion length,  $\lambda_N$ , and so  $\tau_s$ , *via* the usual diffusion relation ( $\lambda_N =$   
 15  $\sqrt{D\tau_s}$ , where  $D$  is the electron diffusivity).

16 These underlying principles of operation have been essential in establishing a consistent  
 17 picture of spin relaxation in NLSVs. Efforts have now largely confirmed that in nanoscopic  
 18 NLSVs based on low SOC metals, relaxation is dominated by the Elliot-Yafet (EY)  
 19 mechanism:<sup>38,39</sup> for a scattering source  $i$  (e.g., phonons, grain boundaries, impurities, *etc.*),  
 20  $1/\tau_{s,i} = 1/\beta_i\tau_{e,i}$ , where  $\tau_{e,i}$  represents the momentum relaxation time due to defect type  $i$ ,  
 21 and  $\beta_i$  is the corresponding EY parameter.<sup>40</sup> Empirically, these rates can be summed using  
 22 what is essentially Matthiessen’s rule for spin transport, to give the total rate:

$$23 \quad \frac{1}{\tau_s} = \sum_i \frac{1}{\beta_i\tau_{e,i}}. \quad (1)$$

1 While a general consensus has emerged supporting this relationship, deconvoluting  
2 contributions from specific mechanisms, i.e., determining each  $\beta_i$ , has been a considerable  
3 challenge, with, for example, an order of magnitude variation in measurements of the phonon  
4 contribution ( $\beta_{ph} = 500 - 3570$ ) extracted from Cu NLSVs.<sup>13-15,41</sup>

5 A primary source of difficulty in this regard is the surprising non-monotonicity of  $R_{spin}(T)$   
6 [or equivalently  $\Delta R_{NL}(T)$ ] at low  $T$ , particularly in Cu-based NLSVs.<sup>7,8,10,19,21,36</sup> In such  
7 devices the extracted  $1/\tau_s$  is found to unexpectedly *increase* at low  $T$ , despite  $1/\tau_e$  remaining  
8 essentially constant, i.e., a striking departure from naïve application of the EY model. Recent  
9 works, by ourselves and others, have shown clear evidence that this is a manifestation of the  
10 Kondo effect, originating from the presence of magnetic impurities (MIs) in the NM  
11 channel,<sup>6,13,41-46</sup> even at very low ( $< 100$  ppm) concentrations. Additionally, we have shown  
12 that the measured spin polarization,  $\alpha$ , is suppressed from its intrinsic value by MIs near the  
13 FM/NM interface.<sup>44</sup> Systematic investigation has shown that the increase in  $1/\tau_s$  and  
14 suppression of  $\alpha$  follow the expected MI concentration scaling<sup>13,42,47-49</sup> and logarithmic  $T$   
15 dependence of the Kondo effect, with a characteristic temperature in good agreement with the  
16 known Kondo temperature ( $T_K$ ) of the Cu/FM pairing.<sup>46</sup> More recently, we have also shown  
17 that Kondo spin relaxation can, surprisingly, be subsumed into an EY form, with an extremely  
18 low effective  $\beta_K = 3/2$ ,<sup>43,44</sup> making MI spin relaxation highly efficient. [*cf.* phonon  $\beta_{ph} =$   
19  $(740 \pm 200)$  and grain boundary  $\beta_{GB} = (240 \pm 50)$  in MI-minimized NLSVs<sup>41</sup>].

20 Interestingly in the context of the above, there is surprisingly clear evidence that a (high)  
21 field enhancement of  $R_{NL}$  exists in certain (e.g., Ag/NiFe<sup>6,26</sup> and Cu/Fe<sup>46</sup>) metallic NLSVs at  
22 low  $T$ . These indications of a non-constant  $R_{spin}(H)$  are significant as they risk undermining  
23 much of the previously established knowledge of spin transport in NLSVs. Specifically, a key  
24 tenet of NLSV operation is that  $R_{spin}$  (or  $\Delta R_{NL}$ ) reliably measures *only* the spin signal and is,

1 for example, field-independent (when the magnetizations of the contacts are parallel to the  
 2 field). Understanding the origin of this field enhancement is the main focus of this work. As an  
 3 example, Fig. 1(c) shows  $R_{NL}(H)$ , taken under identical conditions to that of Fig. 1(b), but now  
 4 over a larger applied field range of  $\pm 9$  T. The field steps used here ( $\sim 100$  mT) are larger than  
 5 the FM coercivities ( $< 60$  mT), so the low  $H$  switching seen in Fig. 1(b) is no longer visible.  
 6 The low coercivity ensures that both contacts are parallel over the entire measurement span, so  
 7 we designate this curve  $R_{NL}^P(H)$ .  $R_{NL}^P$  is clearly not constant, however, with a monotonic  
 8 increase found on increasing  $|H|$ .  $R_{spin}$  is indicated schematically in Fig. 1(c), from which it  
 9 is apparent that the field enhancement is *substantial* compared to the original low-field spin  
 10 signal, in many cases exceeding  $R_{spin}$  in Cu/Fe devices. We define this field enhancement,  
 11  $\delta R_{NL}(H)$  as the difference between  $R_{NL}^P$  at zero field and at a given field  $H$ :

$$12 \quad \delta R_{NL}(H) = R_{NL}^P(H) - R_{NL}^P(0). \quad (2)$$

13 A rigorous explanation of this low  $T$  effect has remained largely elusive. Multiple works have  
 14 investigated qualitatively similar observations, but none can consistently explain all trends. The  
 15 most directly comparable studies,<sup>6,26</sup> using all-metal Ag/NiFe NLSVs, ascribe the field  
 16 dependence to screening of scattering from paramagnetic MIs or magnetic clusters, due to  
 17 alignment with an applied field. Correlating this picture with the  $T$  and  $H$  dependence of  
 18  $R_{NL}(H)$  has been problematic, however, with a lack of ideal agreement between data and  
 19 models based on  $S = 1/2$ , Brillouin-like scaling with temperature and field.

20 In this work we perform an extended investigation into the field-dependence of  $R_{NL}$  in  
 21 metallic NLSVs. By varying the FM (Fe, Co, Ni<sub>80</sub>Fe<sub>20</sub>) and NM (Cu, Al) pairings, we  
 22 demonstrate that the magnitude of  $\delta R_{NL}(H)$  is clearly linked to the ability of the NM to host  
 23 MIs. In Al, where local magnetic moments are not supported on 3d transition metal  
 24 impurities,<sup>47-49</sup> no high-field dependence of  $R_{NL}$  is found. In Cu, where the effect is strong,

1 measurements of  $\delta R_{NL}$  as a function of  $d$ ,  $T$  and  $H$  reveal an isotropic field dependence with a  
2 complex  $T$  and  $d$  relationship. However, taking the critical step of linking  $\delta R_{NL}$  to  
3 enhancement of  $R_{spin}$  allows us to extract values for  $\lambda_N(H, T)$  and  $\tau_s(H, T)$  using standard  
4 spin diffusion theory. Extending spin transport models to incorporate Kondo  
5 magnetoresistance theory, we then demonstrate excellent quantitative agreement between the  
6 experimental  $1/\tau_s(H, T)$  and Kondo spin relaxation theory. A physical picture thus prevails  
7 where the application of  $H$  suppresses MI scattering, restoring the expected  $T$  dependence and  
8 magnitude of the non-local spin signal. As well as solving the long-standing mystery as to the  
9 origin of this low- $T$  field enhancement effect, this high field signature therefore acts as a  
10 convenient method to distinguish spin relaxation due to MIs in metals. We also note that failure  
11 to account for this effect can potentially significantly impact spin transport measurements and  
12 conclusions, particularly in Hanle spin precession experiments, and should thus be  
13 incorporated into future analyses.

14

15

## II. SAMPLE FABRICATION AND EXPERIMENTAL DETAILS

16 NLSV devices were fabricated using multi-angle electron beam evaporation through a  
17 suspended shadow mask. The masks consisted of a polymethylglutarimide (PMGI)/  
18 polymethyl methacrylate (PMMA) bilayer resist stack and were written using a Vistec  
19 EPBPG5000+ electron beam lithography tool, on Si/Si-N (2000 Å) substrates. FM materials  
20 were deposited at an angle of  $49^\circ$  normal to the plane of the device at a rate of  $0.5 \text{ \AA/s}$ . NM  
21 materials were deposited normal to the plane of the device at a rate of  $1.0 \text{ \AA/s}$ . Nominal purities  
22 of the FM and NM materials were 99.95% and 99.999% respectively. All materials were  
23 deposited in the same vacuum system, with a base pressure of the order of  $\sim 10^{-10}$  Torr.  
24 Deposition pressures were in the range  $8 \times 10^{-10}$  to  $4 \times 10^{-8}$  Torr. Thicknesses were calibrated

1 using grazing incidence x-ray reflectivity and monitored during growth using quartz crystal  
 2 monitors. A nucleation pad on one of the FM contacts in each device was used to assist domain  
 3 wall nucleation, reducing the coercivity of that contact, making the antiparallel state more  
 4 readily achievable. NM and FM thicknesses were 200 nm and 16 nm, respectively, for all  
 5 devices, and widths ( $\sim 200$  nm and  $\sim 100 - 150$  nm respectively) were obtained directly from  
 6 SEM measurements. All devices were annealed at  $80^\circ\text{C}$  during processing.<sup>42</sup>

7 Local resistivity measurements were first used to obtain the FM and NM resistivities,  $\rho_{FM}$   
 8 and  $\rho_N$ , and verify the transparent interface limit at the FM/NM interface. Momentum  
 9 scattering rates due to defects  $1/\tau_{e,def}$  and phonons  $1/\tau_{e,ph}$  were calculated from these  
 10 resistivity measurements using  $\rho_N^{-1} = \frac{1}{3} e^2 N(\epsilon_F) v_F^2 \tau_e$ , where  $e$  is the electron charge,  $N(\epsilon_F)$   
 11 the Cu density of states at the Fermi energy, and  $v_F$  the Fermi velocity, with  $\rho_{def}$  estimated  
 12 from the 5 K data. Transport measurements were taken using a 13 Hz AC supply at bias currents  
 13 from 100  $\mu\text{A}$  to 1 mA. A 3  $\mu\Omega$  noise floor was present in the  $R_{NL}$  measurements. At high  
 14 temperatures ( $> 200$  K) and large  $d$  ( $> 1500$  nm), the  $R_{NL}$  signal was dominated by this noise  
 15 floor. An 8% uncertainty in device dimensions was also present.

16

17

### III. RESULTS

18

#### A. Material dependence of $\delta R_{NL}$

19 To-date, only limited combinations of FM and NM materials (Cu/Fe<sup>46</sup> and Ag/NiFe<sup>6,26</sup>) have  
 20 been tested in all-metal NLSVs at relatively high fields. Here, we expand this parameter space  
 21 through NLSVs fabricated using Fe, Co and Ni<sub>80</sub>Fe<sub>20</sub> as the FM, and Cu or Al as the NM. The  
 22 field dependence of  $\delta R_{NL}$  for different material combinations is shown in Fig. 2 and represents  
 23 a key result of our work. Data are shown here for devices with  $d = 250$  nm, at  $T = 5$  K and,  
 24 for direct comparison, they are normalized by  $R_{spin}$  in order to compensate for differences in,

1 e.g., FM current polarization,  $\alpha$ , and FM (NM) resistivity,  $\rho_{FM}$  ( $\rho_N$ ), etc. We first highlight the  
2 Cu/Fe case (red squares). These are the equivalent data to those in Fig. 1(c), once again showing  
3 a monotonic increase in  $\delta R_{NL}/R_{spin}$  up to the largest fields accessible ( $\mu_0 H = 9$  T). Inspection  
4 across all other samples shows an approximately similar curve shape to these Cu/Fe data, with  
5  $\delta R_{NL}$  monotonically rising, well beyond the saturation magnetization,  $M_s$ , of the respective  
6 FMs ( $M_s < 2$  T in all cases, ruling out FM contact rotation as a contributing factor). Comparing  
7 devices, however, clear differences in the normalized magnitude of  $\delta R_{NL}$  are evident. Looking  
8 first at the Cu/Co, Cu/Fe and Cu/Ni<sub>80</sub>Fe<sub>20</sub> devices, it is clear that a large variation in  
9  $\delta R_{NL}/R_{spin}$  occurs across the choice of FM materials. Equally, considering Cu/Fe and Al/Fe,  
10 a noticeable dependence on the choice of NM material is found: whereas a large  $\delta R_{NL}/R_{spin}$   
11 is seen in Cu/Fe devices, almost no field dependence is observed for Al/Fe. The  $\delta R_{NL}/R_{spin}$   
12 behavior is thus dependent on *both* the FM *and* NM material choices.

13 Similar field-dependent trends are also found in other spintronic devices, including three  
14 terminal spin valve measurements of semiconductors,<sup>50</sup> hydrogenated graphene NLSVs,<sup>51</sup> and  
15 heavy metal magnetoresistance measurements,<sup>52</sup> attributed to precession from inhomogeneous  
16 magnetostatic fields, local moment exchange interactions, or Hanle precessional  
17 magnetoresistance, respectively. In the case of light metal NLSVs, the non-local measurement  
18 (limiting the impact of contact relaxation), metallic nature of the transport, extended field  
19 dependence ( $>9$  T), and low SOC (and spin Hall angle) rules out each of these explanations.

20 Instead, as with earlier work on MI effects in spin transport, we return to the stark correlation  
21 between the ability of the host NM to support MIs arising from the FM, and (in this case) the  
22 magnitude of  $\delta R_{NL}(H)$ . Specifically, Cu readily hosts local magnetic moments on dissolved  
23 3d transition metal impurities, whereas Al (primarily due to its high Fermi level) does not,<sup>47-49</sup>  
24 a trend that is precisely reflected in the magnitudes observed in Fig. 2. This is further supported



1 by  $\delta R_{NL}/R_{spin}$  in Al interlayer (Al-IL) devices, where a thin ( $\sim 5\text{nm}$ ) layer is deposited between  
 2 the Cu and Fe layers. Due primarily to the low diffusivity of Fe in Al, the Al-IL greatly reduces  
 3 the concentration of Fe impurities in the channel. As a consequence, Cu/Al-IL/Fe devices  
 4 exhibit a weak (but non-zero) high field dependence.

### 5 **B. Determining the origin of $\delta R_{NL}$**

6 A natural implication of this correlation between local moment formation and the high field  
 7 dependence is that  $\delta R_{NL}$  arises from a spin transport effect, related to MI-driven spin  
 8 relaxation. Before continuing with a MI-based analysis, including detailed comparison between  
 9 datasets, we first consider other potential phenomena, unrelated to spin transport, as the  
 10 potential origins of  $\delta R_{NL}(H)$ , e.g., field-dependent thermoelectric<sup>33,34,53</sup> or current spreading<sup>32</sup>  
 11 effects. In such cases,  $\delta R_{NL}$  would be expected to correlate broadly with the field-independent  
 12 background  $R_b = (R_{NL}^P + R_{NL}^{AP})/2$ , in sign, magnitude,  $d$  or  $T$  dependence.

13 To test this, in Fig. 3(a) and (b), we show the temperature evolution of  $\delta R_{NL}$  and  $R_b$  for  
 14 Cu/Fe NLSVs of varying  $d$ , and provide a direct comparison of the two in Fig. 3 (d). Examining  
 15 Fig. 3(a) and (b), we note that the magnitude of  $\delta R_{NL}$  is relatively large, at times exceeding  
 16 that of  $R_b$  and  $R_{spin}$  [shown in Fig. 3(c)]. Field-dependent corrections to  $R_b$  from current  
 17 spreading, of order  $\omega_c \tau_e$  (where  $\omega_c$  is the cyclotron frequency)<sup>32</sup>, are weak in comparison [at  
 18 most of the order  $10^{-2}$  at 9 T for our longest measured  $\tau_e \approx 50$  fs ( $T = 5$  K)]<sup>32</sup>, ruling out current  
 19 spreading as the origin of  $\delta R_{NL}$ . Further examining Fig. 3(a) and (b), it is also clear that there  
 20 is no correlation between the evolution of  $\delta R_{NL}$  and  $R_b$ : Whereas  $\delta R_{NL}$  decreases with both  
 21 increasing  $T$  and  $d$  (Fig. 3(a)),  $R_b$  appears largely independent of these parameters in Cu/Fe  
 22 (Fig. 3(b)). Comparing different materials pairings (as shown in Supplemental Material Fig.  
 23 S1<sup>54</sup>) yields further inconsistencies in the signs and magnitudes of  $\delta R_{NL}$  and  $R_b$ , which are  
 24 incompatible with the possibility that  $\delta R_{NL}$  arises from current-spreading or thermoelectric

1 effects. Thus, we can convincingly rule out contributions from conventional (non-spin)  
2 transport phenomena, which otherwise determine  $R_{\beta}$ .

3 We next consider magnetothermoelectric (e.g., a field-dependent spin-Seebeck  
4 contribution), or weak (anti)localization effects, which are anisotropic with respect to the  
5 applied field direction.<sup>27</sup> Comparing  $R_{NL}(H)$  for different field directions, as in Fig. 3(f),  
6  $\delta R_{NL}(H)$  is found to be isotropic with respect to the direction of the applied field. Here, we  
7 compare  $R_{NL}(H)$  for in-plane ( $H_y$ ) and out-of-plane ( $H_z$ ) magnetic fields at  $T = 5$  K (other  
8 temperatures are shown in Supplemental Material Fig. S2<sup>54</sup>). Out-of-plane measurements are  
9 shown for initial parallel and anti-parallel alignment of the FM contacts, and are essentially  
10 Hanle effect measurements: the oscillations in  $R_{NL}$  thus arise from Larmor precession of  
11 conduction electron spins about  $H_z$ , decaying as the magnetizations of  $FM_{inj}$  and  $FM_{det}$  rotate  
12 to align with the field. These in-plane and out-of-plane measurements were taken at different  
13 times, and inevitably there is a small difference in the zero-field offset to  $R_{NL}$ . For ease of  
14 comparison, the offset in the in-plane measurements has been shifted (by  $\sim 30 \mu\Omega$ ), to match  
15 that of the parallel, out-of-plane measurement at zero field. Beyond the saturation field of the  
16 FM contacts (1.8 T), the out-of-plane  $R_{NL}$  for both parallel and anti-parallel orientations  
17 increase exactly as the in-plane  $R_{NL}$  does. This is to say that  $\delta R_{NL}(H)$  is independent of the  
18 direction of applied field, and therefore does not originate from magnetothermoelectric, weak  
19 (anti)localization effects, nor current spreading, which would all have an anisotropic  
20 dependence on field direction.<sup>27,28</sup>

21 In contrast, for a given NM/FM pairing, we find that  $\delta R_{NL}(\mu_0 H = 9 \text{ T})$  broadly scales with  
22 the magnitude of  $R_{spin}$  (see Figs. 3(a), (c) and (e) for Cu/Fe, and Supplemental Material Fig.  
23 S1<sup>54</sup> for Cu/Co, Cu/Ni<sub>80</sub>Fe<sub>20</sub> and Al/Fe). While the specific dependence of  $\delta R_{NL}(T, d)$  is  
24 complex, and  $\delta R_{NL}/R_{spin}$  varies between pairings, for a given FM and NM,  $\delta R_{NL}(H)$

1 decreases on reduction of  $R_{spin}$ , either through increasing  $T$  or  $d$  (Fig. 3(e)). From this we  
2 conclude that  $\delta R_{NL}(H)$  has a similar dependence on the spin-dependent parameters of each  
3 material, and indeed arises from a pure spin transport effect.

4 We next examine the  $T$  dependence of  $\delta R_{NL}(H)$ . Cu/Fe offers one of the largest field  
5 enhancements, and so we focus on this pairing. (Cu/Fe also provides a convenient pairing for  
6 testing Kondo-related contributions, due to its relatively high miscibility and an easily  
7 accessible  $T_K = 30$  K<sup>47</sup>). Fig. 4 displays  $\delta R_{NL}(H)$  for a Cu/Fe device with  $d = 250$  nm, across  
8 a  $T$  range of 5-250 K. As well as increasing with field,  $\delta R_{NL}$  clearly decreases with increasing  
9  $T$ . Qualitatively, such scaling is commensurate with the saturation of paramagnetic MI  
10 moments under increasing field or decreasing temperature. However, plotting the normalized  
11  $\delta R_{NL}$  vs.  $\mu_B \mu_0 H / k_B T$  (inset) fails to collapse the data onto a single functional form, as might  
12 be anticipated for the response of free moments under field. Furthermore,  $\delta R_{NL}$  shows a  
13  $\mu_B \mu_0 H / k_B T$  dependence that is not only far stronger than expected for  $S = 1/2$  MIs, (for all  
14 but the lowest 5 K data) but is also poorly described by a classical Langevin expression, where  
15 the fitted  $J$  varies dramatically with  $T$  (see Supplemental Material Fig. S3<sup>55</sup>). A similar  
16 observation was made in references 6 and 26, and was attributed to the finite magnetic shape  
17 anisotropy energy of clustered MIs. In our devices similar  $\delta R_{NL}(H)$  is observed across  
18 different material pairings, therefore analysis based on magnetic shape anisotropy would  
19 require similar clustering of MIs across these pairings. However, the range of thermodynamic  
20 solubilities are unlikely to produce identical distributions and precipitations of (potentially  
21 clustered) MIs, seeming to disfavour such a model, and suggesting a fundamentally different  
22 mechanism is at play.

23

24

### C. Extracting spin transport characteristics

Acknowledging that  $\delta R_{NL}$  arises from a spin transport effect, we must accept that any changes in  $\delta R_{NL}(T)$  are manifestly convolved with the  $T$ -dependent variation of the key relevant NLSV material parameters, particularly  $\tau_s(T)$ ,  $\alpha(T)$ ,  $\rho_N(T)$  and  $\rho_{FM}(T)$ . Given that all other key parameters are either constant ( $d$ , and the NM thickness,  $t_N$ ) or have a weak  $H$  dependence ( $\rho_N$ ,  $\rho_{FM}$ ,  $\lambda_F$ ), we proceed by considering the (MI) scattering contribution to  $\tau_s$  and  $\alpha$ , which are now anticipated to depend on  $H$ , as well as  $T$ . To extract these terms, a comprehensive study of  $R_{NL}(H)$  in Cu/Fe NLSVs was performed at various  $d$  (250-2000 nm) and  $T$  (5-250 K).

Reasoning that the field dependence of  $R_{NL}$  can be subsumed into  $\tau_s$  and  $\alpha$  is equivalent to defining a field-dependent NLSV spin signal,  $R_{spin}(H) = R_{spin}(0) + \delta R_{NL}(H)$ , where  $R_{spin}(0) = R_{NL}^P(0) - R_b$  as defined earlier. This model is based on the assumption that  $R_b$  is independent of the magnetic field, which is easily verified following our discussion in Sec. III. B. To calculate  $R_{spin}(H)$ , we obtained  $\delta R_{NL}(H)$  data for a range of  $T$  and  $d$  values, via equation 2. Because it is convenient to be able to represent the data as a continuous function of  $H$ , we adopt for now a purely empirical fitting function:

$$\delta R_{NL}(H) = \left| A_1 \left( \coth x - \frac{1}{x} \right) \right| - A_2 |\mu_0 H| \quad (3)$$

where  $x = \mu_0(H - H_0)/b$ , and  $A_1$ ,  $A_2$ ,  $b$  and  $H_0$  are constant fitting parameters. We emphasize that our use of equation (3) is solely as a representation of the data, and offers little physical insight. The fitted curves (shown by the solid lines in Fig. 4) are combined with measurements of  $R_{spin}(0)$  to obtain  $R_{spin}(H)$  for any given field within  $\pm 9$  T, and at selected  $d = 250$ -2000 nm and  $T = 5$ -250 K. Representative values of  $R_{spin}(d, H)$  are shown in Fig. 5(a) for  $\mu_0 H = 0, 1, 3, 5$  and 9 T, at  $T = 5$  K. Despite the varying magnitude of  $\delta R_{NL}$  vs.  $H, T$

1 and  $d$ ,  $R_{spin}(d, H)$  assumes the expected functional form for all  $H$ : a simple exponential decay  
 2 at high  $d$  with the deviation at low  $d$  that is a hallmark of NLSV spin diffusion in the low  
 3 interface resistance limit. Encouraged by this  $d$  dependence, we fit these data using a standard  
 4 1-D magnetoelectronic circuit theory solution for  $R_{spin}(H)$ , applied to the NLSV geometry in  
 5 the transparent interface limit:<sup>56</sup>

$$6 \quad R_{spin}(H) = 2 \frac{\alpha_{eff}^2 R_F^2}{(1 - \alpha_{eff}^2)^2 R_N} \frac{\exp\left(-\frac{d}{\lambda_N}\right)}{\left[1 + \frac{2R_F}{(1 - \alpha_{eff}^2)R_N}\right]^2 - \exp\left(-\frac{2d}{\lambda_N}\right)}. \quad (4)$$

7 Here,  $R_N = \rho_N \lambda_N / w_N t_N$  and  $R_F = \rho_F \lambda_F / w_F w_N$  are the NM and FM spin-resistances, with  
 8  $\rho_N$  ( $\rho_F$ ) and  $w_N$  ( $w_F$ ) the respective resistivities and widths; and  $t_N$  the NM thickness. In  
 9 equation (4) we employ an effective spin polarization,  $\alpha_{eff}$ , to account for the presence of MI-  
 10 induced depolarization at the NM/FM interfaces<sup>42</sup> and to distinguish it from the intrinsic FM  
 11 polarization,  $\alpha$ . To constrain the fitting, we experimentally measure  $\rho_N$  on the same NLSVs,  
 12 and  $\rho_F$  on nanowires of identical cross-sectional dimensions. All dimensions were measured  
 13 using SEM for each device, and  $\lambda_F$  was constrained to a value of 4 nm through empirical  
 14 scaling with  $\rho_F$ .<sup>46,57</sup> Only  $\lambda_N$  and  $\alpha_{eff}$  thus remain as fitting parameters, and these two are  
 15 readily separable through the high- $d$  exponential dependence, which is determined only by  $\lambda_N$ .  
 16 Extracted values of  $\lambda_N(T)$  for selected field values are shown in Fig. 5(b), along with the  
 17 corresponding  $1/\tau_s(T)$  (through the diffusion relation,  $\lambda_N = \sqrt{D\tau_s}$ ) in Fig. 5(c). In Fig. 5(d)  
 18 the relevant  $\alpha_{eff}(T)$  are displayed.

#### 19 **D. Temperature and field dependence of spin transport**

20 Looking first at the zero-field  $\lambda_N(T)$  data in Fig. 5(b), an initial increase in  $\lambda_N$  with decreasing  
 21  $T$  is observed from 250 K to 40 K, as phonon scattering is progressively frozen out. Below 40  
 22 K a noticeable downturn is then observed, producing a peak in  $\lambda_N(T)$ . This peak, widely seen

1 in other works<sup>7,8,11,21</sup>, and clearly contrasting with the naïvely expected (monotonic) EY-like  
 2 behaviour,<sup>40,58</sup> is qualitatively similar to that seen in low-purity Cu/Fe NLSVs.<sup>41,42,46</sup> There, it  
 3 is attributed to Kondo relaxation arising from dilute MIs, present throughout the channel (even  
 4 in initially high-purity NM materials, NM/FM interdiffusion will inevitably introduce MIs into  
 5 the channel if the solubility is high enough). We note that, at low  $T$ ,  $\lambda_N$  should approach a  
 6 constant value due to the unitary limit of Kondo relaxation. As shown in our previous work,  
 7 this is readily observed in our devices when  $T \ll 30$  K,<sup>46</sup> and is particularly prevalent in devices  
 8 with high MI concentrations and/or higher Kondo temperatures<sup>42,45</sup>. Indeed this effect is also  
 9 evident here, although the coarser  $T$  steps limit quantitative comparison.

10 Although on first inspection the downturn in  $\lambda_N(T)$  is a seemingly weak effect, we emphasize  
 11 that the full impact of MI relaxation can only be assessed from the departure from conventional  
 12 spin relaxation due to phonon and  $T$ -independent defect scattering alone. To demonstrate this,  
 13 we estimate the expected  $1/\tau_s(T)$  and  $\lambda_N(T)$  for EY-type scaling, using equation (1) for  
 14 phonon and defect scattering.  $1/\tau_{e,def}$  and  $1/\tau_{e,ph}$  are calculated as described in Sec. II, and  
 15 we use typical values for phonon and defect EY parameters,  $\beta_{ph} = 740$  and  $\beta_{def} = 240$ ,  
 16 respectively, previously determined from devices in which MI effects were minimized.<sup>41</sup>  
 17 (Under such conditions, grain boundaries were found to dominate defect scattering, and so we  
 18 use  $\beta_{def} = \beta_{GB}$ .)  $\lambda_N$  values were then calculated from  $1/\tau_s$  using the diffusion relation  $\lambda =$   
 19  $\sqrt{\tau D}$ , where  $D$  is the diffusivity taken from local resistivity measurements. The corresponding  
 20 curve, represented by the black dashed line in Fig. 5(b), demonstrates the stark impact of MI  
 21 spin relaxation, which results in  $\sim 30\%$  suppression of  $\lambda_N$  at 5 K. In this context, the impact of  
 22 applying  $H$  becomes clearer. Specifically, examining  $\lambda_N(T)$  with increasing  $H$  we find a simple  
 23 trend where  $\lambda_N(T)$  steadily rises until it approaches the very same monotonic dependence  
 24 expected in Kondo-minimized devices. We conclude, therefore, that the field acts to quench  $T$ -  
 25 dependent MI (i.e., Kondo) scattering.

1      Equivalent behavior is observed in  $1/\tau_s$ , as shown in Fig. 5(c), where the  $H = 0$  scattering  
 2 rate initially decreases with  $T$ , down to 90 K, before unexpectedly increasing on further  
 3 cooling. Both the magnitude and  $T$  dependence of this behaviour are in good agreement with  
 4 the  $1/\tau_s$  seen in other Cu/Fe devices<sup>41,42,46</sup>, but once again strongly contrasts with expected EY  
 5 theory (black dashed curve). At this point we note that in the Kondo model,  $T_K$  determines a  
 6 characteristic temperature scale about which the scattering rate becomes enhanced, rather than  
 7 any critical temperature. The increase in  $1/\tau_s$  about  $T \sim 25$  K is therefore consistent with the  
 8 onset of the Kondo effect in Cu/Fe ( $T_K = 30$  K).<sup>46,47,59</sup> While this upturn in  $1/\tau_s$  at low  $T$  has  
 9 now been widely observed, the restoration of  $1/\tau_s$  under increasing  $H$  is new here and is stark.  
 10 Under application of the field,  $1/\tau_s$  approaches the expected EY dependence, which is nearly  
 11 restored by  $\mu_0 H = 9$  T. Despite the action of  $H$  in quenching Kondo scattering, a noticeable  
 12 shoulder remains at low  $T$ , even at  $\mu_0 H = 9$  T. As we will detail below, this shoulder is a  
 13 hallmark of such MI scattering, and is produced by the competition between different energy  
 14 scales in the system, notably the Kondo singlet, thermal and Zeeman energies.

15      We next consider these observations further by comparing Cu/Fe with other NM/FM  
 16 combinations. While we do not make in-depth quantitative comparison, we do examine the  
 17 (normalized) residual scattering rate,  $1/\tau_{s,res} = 1/\tau_s^{zero\ field} - 1/\tau_s^{high\ field}$ , for Cu/Co,  
 18 Cu/NiFe and Cu/Fe, where “high field” refers to the highest field available (4.5 T for Cu/Co, 9  
 19 T otherwise).<sup>54</sup> From the preceding discussion, in essence,  $1/\tau_s^{high\ field}$  corresponds to the  
 20 relaxation rate under the near-complete quenching of MI scattering, but without any changes  
 21 to  $1/\tau_{s,ph}$ . Defined in this way,  $1/\tau_{s,res}(T)$  can therefore provide an estimate of the  $T$ -  
 22 dependence of MI scattering, although it cannot give insight into its overall magnitude.  
 23 Additionally, the absolute value of  $1/\tau_{s,res}$  is dependent on the material properties of the

1 FM/NM pairings, and so, for suitable comparison between pairings, we normalize the data to  
 2 their maximum value.

3 The normalized  $1/\tau_{s,res}(T)$  data are shown in Fig. 6, on a logarithmic temperature scale. In  
 4 all cases, as expected,  $1/\tau_{s,res}$  decreases with temperature. Significantly, Cu/Fe shows a clear  
 5 logarithmic  $T$  dependence about a temperature range consistent with  $T_K = 30$  K. As this data  
 6 set is quite complete, we fit the data using the phenomenological Goldhaber-Gordon expression  
 7 for Kondo scattering<sup>60</sup>:

$$8 \quad \frac{1}{\tau_{s,res}} = G_0 \left[ \frac{T_K'^2}{T^2 + T_K'^2} \right]^s \quad (5)$$

9 where  $T_K' = T_K/\sqrt{2^{1/s} - 1}$  and  $s = 0.22$  for spin-1/2 MIs<sup>46,60</sup>. Since the data are normalized,  
 10 we fix  $G_0 = 1$  and  $T_K$  remains as the only free parameter. The fit (solid line) models the data  
 11 reasonably well, returning  $T_K = (20 \pm 8)$  K, in decent agreement with the expected  $T_K = 30$  K.  
 12 Encouragingly, this Cu/Fe behavior is reproduced in Cu/Ni<sub>80</sub>Fe<sub>20</sub> (Ni is not expected to show  
 13 any Kondo contribution due to the prohibitively high  $T_K \sim 1000$  K, thus only Fe moments  
 14 should contribute for Cu/Ni<sub>80</sub>Fe<sub>20</sub>). In contrast, Cu/Co has a response which is clearly shifted  
 15 to higher  $T$ , appearing to reach the unitary limit at  $T \sim 50$  K. This correlates well with the  
 16 increased  $T_K$  value for this pairing (Cu/Co has a  $T_K$  of either 23 or 500 K depending on whether  
 17 the MIs are surface or bulk, respectively<sup>46,61</sup>), further cementing the relationship between  
 18  $\delta R_{NL}(H)$ , through  $1/\tau_s$ , and MI scattering.

### 19 **E. Fitting the spin relaxation rate, $1/\tau_s$**

20 Given the success of Kondo scattering in qualitatively describing  $1/\tau_s(T)$  for Cu/FM NLSVs,  
 21 we continue this approach, now quantitatively accounting for the impact of  $H$  on  $\tau_{s,K}$ . Previous  
 22 studies of the magnetoresistance of Cu<sub>1-x</sub>Fe<sub>x</sub> and similar alloys have shown that application of  
 23 a magnetic field indeed suppresses Kondo scattering at low temperatures,<sup>62,63</sup> and several



1 qualitatively similar models have been proposed<sup>64–66</sup>. Here, we use the model derived by  
 2 Litvinov,<sup>64</sup> which most accurately represents Fe impurities in a metallic host. (We have also  
 3 performed analysis using the Abrikosov model<sup>65</sup>, which we present in the Supplemental  
 4 Material Fig. S4; similar results are produced.<sup>67</sup>) In the Litvinov theory, the Kondo momentum  
 5 scattering rate is given by:

$$6 \quad \frac{1}{\tau_{e,K}} = \frac{3\pi c J^2}{32\hbar\varepsilon_F} \times \frac{2 \tanh\left(\frac{Q}{k_B T}\right) - \tanh\left(\frac{Q}{2k_B T}\right)}{\sinh\left(\frac{Q}{k_B T}\right)} \times \left[1 + \frac{3J}{4\varepsilon_F} \ln\left(\frac{k_B T_K^2}{(2k_B T)^2 + Q^2}\right)\right]^{-2} \quad (6)$$

7 where  $c$  is the concentration of magnetic impurity atoms,  $J$  is the exchange energy between the  
 8 magnetic impurity and conduction electrons, and  $\varepsilon_F$  is the Fermi energy.  $Q = \mu_0\mu_B g_i H$  is the  
 9 Zeeman energy due to the magnetic field, where  $g_i$  is the impurity  $g$ -factor (assumed to equal  
 10 2). There are two energy scales at play in this equation: the first, which comprises the  
 11 hyperbolic terms, describes the magnetization of the magnetic impurities and the competition  
 12 between  $T$  and  $H$ ; the second, which is the modified Kondo term, acts to suppress the scattering  
 13 rate, with contributions from the singlet and Zeeman energies.

14 The data in Fig. 5(c) were fit using equations (1) and (6), considering terms from phonon,  
 15  $T$ -independent impurities, and Kondo scattering explicitly. Here,  $1/\tau_{e,ph}$  and  $1/\tau_{e,imp}$  are  
 16 known from local measurements of  $\rho_N$ , while  $J = -0.91$  eV and  $\varepsilon_F = 7.0$  eV may be  
 17 constrained for Fe;<sup>44,62</sup> and  $\beta_K = 3/2$  is known at zero field.<sup>44,68</sup> At  $H \neq 0$ , however,  $\beta_K$  is  
 18 expected to vary: the Zeeman energy of the magnetic field breaks the symmetry of spin-flip  
 19 Kondo scattering, but not of spin-conserving Kondo scattering, resulting in different field  
 20 dependencies and hence a non-constant  $\beta_K(H)$ <sup>66,69,70</sup>. As discussed further below, the fits  
 21 therefore remain underconstrained, with free parameters  $\beta_{def}, \beta_{ph}, c$  and  $\beta_K(H)$ . For  
 22 simplicity, we have employed a constant, volume average impurity concentration in the model,  
 23 although it is expected that  $c$  will vary with distance from the NM/FM interface.<sup>42</sup> Since

1  $\beta_K(H = 0) = 3/2$ , the zero-field data were first fit, returning values of  $\beta_{def} = 230$ ,  $\beta_{ph} = 470$ ,  
2 and  $c = 890$  ppm. From the earlier discussion, these values are clearly physically reasonable,  
3 and fall among those from our prior work, and the work of others.<sup>9,11,15,18,41</sup> As these parameters  
4 are expected to be invariant under  $H$ , they were then used as fixed values for the remaining fits,  
5 with only  $\beta_K(H)$  allowed to vary, significantly constraining the fit. Best fit curves using this  
6 approach are shown at select fields by the solid lines in Fig. 5(c), and the variation of the  
7 extracted  $\beta_K(H)$  is displayed in the inset.

8 It can be clearly seen that this model represents the data well; in particular, the knee observed  
9 between  $T = 5$  and 50 K at higher fields is accurately reproduced. This is a strong indication  
10 that the magnetic field is indeed acting to suppress Kondo scattering in the NM channel, and  
11 that the high field dependence of  $R_{spin}(H)$  can be quantitatively understood through the  
12 quenching of the ( $T$ -dependent) singlet scattering. The behavior of  $\beta_K$  is of particular interest.  
13  $\beta_K$  is expected to increase with increasing  $H$ , as the alignment of the magnetic impurities  
14 freezes out spin-flip Kondo scattering events.<sup>66</sup> However, as far as we are aware, no prior work  
15 has experimentally examined this precise evolution. We thus consider this determination of  
16  $\beta_K(H)$  an important dataset for the future understanding of the Kondo effect and its relationship  
17 with spin relaxation, and we believe it represents a new challenge to theory to accurately model  
18 this observed dependence.

## 19 **F. Field dependence of the effective current polarization, $\alpha_{eff}$**

20 Before concluding, as an additional consistency check we consider the behavior of the effective  
21 current-polarization,  $\alpha_{eff}(H, T)$ , as shown in Fig. 5(d). The  $\alpha_{eff}(T)$  data for Cu/Al-IL/Fe are  
22 also shown here (green diamonds). In the absence of Kondo scattering,  $\alpha_{eff}$  should approach a  
23 constant on cooling, as in the Al-IL device. In the Cu/Fe device however, this is not the case at  
24 small fields: as in the  $\lambda_N$  data, a downturn in  $\alpha_{eff}$  is seen at low temperatures, due to Kondo

1 scattering through interdiffused MIs near the NM/FM interface, which is known to suppress  
 2 the injected spin polarisation.<sup>44</sup> Once again, however, the application of a magnetic field  
 3 removes this suppression, as clearly shown in Fig. 5(d). By  $\mu_0 H = 5$  T,  $\alpha_{\text{eff}}(T)$  is in fact  
 4 approximately restored to that in the Al-IL device. In reference 44, some of us showed that this  
 5  $\alpha_{\text{eff}}$  suppression is described by:

$$6 \quad \alpha_{\text{eff}} = \alpha \left\{ 1 - z \left[ \frac{1 + \frac{2}{\beta_K} \frac{\tau'_S}{\tau'_e}}{\lambda_N} - \frac{\frac{2}{\beta_K} \frac{\tau'_S}{\tau'_e}}{\lambda_N + \frac{\rho_F}{(1 - \alpha^2) \rho_N} \lambda_F} \right] \frac{\tau'_e}{\tau_{e,K}} \right\} \quad (7)$$

7 where  $z$  is the characteristic interdiffusion depth of the magnetic impurities in the NM channel,  
 8 which is expected to be of the order of 10's of nm for Cu/Fe,<sup>42</sup> and  $\tau'_e$  and  $\tau'_S$  are the MI-free  
 9 momentum and spin relaxation times, respectively.  $1/\tau'_e$  and  $1/\tau'_S$  were obtained using  $1/\tau'_e =$   
 10  $1/\tau_e - 1/\tau_{e,K}$  and  $1/\tau'_S = 1/\tau_S - 1/\beta_K \tau_{e,K}$ , where,  $1/\tau_e$  and  $1/\tau_S$  are determined from  $\rho_N$   
 11 and  $\lambda_N$ , while  $1/\tau_{e,K}$  and  $\beta_K$  are the best fit values shown in Fig. 5(c). This leaves  $z$  and the  
 12 intrinsic spin polarization,  $\alpha$ , as the only free parameters in fits. The resulting best fit curves,  
 13 shown by the solid lines in Fig. 5(d), reproduce the  $\alpha_{\text{eff}}$  data well. The extracted values of  $\alpha =$   
 14  $0.4 \pm 0.04$  and  $z = 57 \pm 24$  nm across the data set are also entirely plausible, and comparable to  
 15 values obtained in reference 44.

16 It is evident from these results that the field-dependent background effects in  $R_{NL}$  can be  
 17 understood as the suppression of Kondo scattering in the NM channel. Moreover, by extracting  
 18  $1/\tau_S$  and  $\alpha_{\text{eff}}$  from the  $R_{\text{spin}}(d, T)$  data, the suppression of the Kondo scattering can be  
 19 effectively modelled by the use of equations (6) and (7). This has clear implications for NLSV  
 20 devices based on materials that host MIs and hence have  $\tau_S$  and  $\alpha_{\text{eff}}$  reduced by Kondo  
 21 scattering. This effect is also likely to be present in more complicated systems, such as those  
 22 where MIs have been intentionally introduced, or in complex heterostructures of Kondo active  
 23 pairings. Here, relaxation from MIs could dominate and obscure spin lifetime measurements,

1 e.g., through distortion of Hanle spin precession curves, due to the field dependence of both  
 2 the saturation background and the spin lifetime. However, we have demonstrated in this work  
 3 a simple means to quantify this effect, by application of a magnetic field large enough to  
 4 saturate the moments.

### 5 **G. Exchange field model**

6 Due to the nature of our devices, which contain very low concentrations of dilute MIs, we  
 7 discussed  $R_{spin}(H)$  above in terms of the physically relevant Kondo scattering regime. For  
 8 completeness, however, we may also consider the impact of spin decoherence due to precession  
 9 about a random exchange field, arising from MIs, such as those considered by McCreary *et*  
 10 *al.*<sup>51</sup> In such an exchange field model, the conduction electrons experience an exchange field  
 11 from the impurity moments, with RMS fluctuations,  $\Delta B_{ex}$ , about the average field  $\overline{B_{ex}}$ ,  
 12 occurring on a timescale  $\tau_c$ , the correlation time. The spin relaxation rate due to this exchange  
 13 field is given by:<sup>51,71</sup>

$$14 \quad \frac{1}{\tau_{ex,s}} = \frac{(\Delta B_{ex})^2}{\tau_c} \frac{1}{(\mu_0 H + \overline{B_{ex}})^2 + \left(\frac{\hbar}{g_e \mu_B \tau_c}\right)^2} \quad (8)$$

15 where  $\hbar$ ,  $g_e$  and  $\mu_B$  are Planck's constant, the electron g-factor and the Bohr magneton  
 16 respectively. Following the procedure in reference 51, we assume  $\overline{B_{ex}}$  is described by a  
 17 Brillouin function,  $B_S$ , through

$$18 \quad \overline{B_{ex}} = \frac{cJS}{g_e \mu_B} B_S(\xi) \quad (9)$$

19 where  $\xi \equiv Q/k_B T$ , and  $B_S(x)$  reduces to  $\tanh(x)$  for spin  $S = 1/2$  impurities.

20 We reproduce the spin relaxation rate as a function of temperature in Fig. 7(a), and now  
 21 attempt to fit it with this exchange field model.  $\Delta B$  and  $\tau_c$  are expected to be independent of  
 22 the magnetic field, but should vary with  $T$ , and we therefore fit  $1/\tau_s(H)$  at fixed  $T$  using

1 equations (1), (8) and (9), with  $\Delta B$  and  $\tau_c$  as free parameters. (This is in contrast to the fitting  
2 procedure in Sec. III E, in which we fit  $1/\tau_s(T)$  at fixed  $H$ .)

3 Although the exchange model appears to fit the data well, the extracted  $\Delta B$  and  $\tau_c$  are  
4 revealing. These are shown in Fig. 7(b) and (c) respectively, for  $c = 100$  ppm and 1000 ppm.  
5 We choose 1000 ppm here as this is close to the upper limit of a dilute system, and higher  
6 concentrations would be expected to lead to phase separation of Cu and Fe. Concentrations of  
7 100 ppm and below are likely more representative of our devices, and we find that, at these  
8 concentrations,  $c$  has negligible impact on  $\Delta B$  and  $\tau_c$ , since  $\overline{B_{ex}} \ll \mu_0 H$  in equation (8). Note  
9 that the 250 K  $\Delta B$  and  $\tau_c$  data have been excluded in Fig. 7(b,c), due to anomalously low and  
10 high values, respectively, likely due to the large spread in the  $1/\tau_s$  data at this temperature  
11 (Fig. 7(a)).

12 Looking first at the  $c = 100$  ppm case,  $\Delta B(T)$  is seen to fluctuate about a constant value of  
13  $\sim 1.2$  T. Although possible, such a large magnitude of  $\Delta B$  is unlikely.  $\tau_c$  also exhibits a strong  
14 temperature dependence, increasing with decreasing  $T$ , indicative of what would occur at a  
15 spin glass transition, for example. It is generally expected that  $\tau_c$  is constant in both NM and  
16 FM materials, changing dramatically only during a phase transition, e.g., spin glass  
17 freezing.<sup>47,72-74</sup> Given the dilute nature of the MIs here, and so the weak inter-MI coupling, we  
18 do not believe that this  $T$  dependence can be physically realistic, particularly as we are far from  
19 the concentrations required for a spin glass transition at this temperature ( $c \sim 1\%$  for a  
20 transition at around 10 K in  $\text{Cu}_{1-x}\text{Fe}_x$ ).<sup>75,76</sup>

21 Although unlikely, we nevertheless test the hypothesis of  $\tau_c(T)$  indicating a spin glass  
22 transition using the conventional description for the critical slowing down of spin dynamics in  
23 a spin glass<sup>47,77</sup>:

$$\tau_C = \tau_0 \left( \frac{T - T_g}{T_g} \right)^{-z\nu} \quad (10)$$

where  $T_g$  is the spin glass transition temperature,  $\tau_0$  is a characteristic timescale and the exponent  $z\nu$  is a constant. We fit the data using equation (10), with  $\tau_0$ ,  $T_g$  and  $z\nu$  as free parameters. The resulting fit, shown in Fig. 7(c), models the data reasonably, but fails to completely reproduce the form of  $\tau_C(T)$ . Moreover, the extracted parameters are  $T_g \approx 0$  K and  $z\nu = 0.25$ . Such a  $z\nu$  value is unfeasibly low,<sup>47</sup> indicating that we are far from a transition at a (finite)  $T_g$  near 0 K. It is therefore unlikely that such a spin glass transition is occurring in our devices.

Moving to the behavior of  $\Delta B$  and  $\tau_C$  at  $c = 1000$  ppm, we find even less physical behavior, with  $\Delta B$  increasing on cooling to a very large 2.7 T at 5 K, and  $\tau_C$  varying non-monotonically with  $T$ . Such a strong temperature dependence of  $\Delta B$ , and large magnitude, is clearly unreasonable. Hence, although the exchange model is able to fit the  $1/\tau_S$  data, it is not able to provide satisfying physical insight into the  $T$  and  $H$  variation of  $1/\tau_S$  (and thus  $\delta R_{NL}$ ), as evidenced by the unreasonable  $T$  dependencies of  $\Delta B$  and  $\tau_C$ . We therefore conclude that the exchange model is not a suitable description for the field enhancement of  $R_{NL}$  we observe in our devices. We do emphasize, however, that this does not rule out such a mechanism becoming active in devices where the NM is (intentionally) more heavily substituted with MIs (thereby introducing MI-MI interactions) or directly exchange-coupled to a FM.<sup>31</sup> There, it is reasonable to assume such exchange field coupling could be active. Indeed, should the materials in these devices undergo a magnetic phase transition, e.g., FM ordering or spin glass freezing, then it is reasonable to expect this will also contribute to non-monotonicity in  $R_{spin}(H, T)$ , potentially with comparable magnitudes to the Kondo scattering observed here. These could potentially be identified through the characterization of  $T_g$  and  $z\nu$ .

## IV. CONCLUSION

An increase in non-local resistance in NLSVs under the application of an external magnetic field has been previously reported,<sup>6,26</sup> and is observed here. Through the experimental measurement of a wide range of metallic NM/FM combinations, we demonstrate that the effect is correlated with the ability of the NM metal to host dilute magnetic impurity moments. Considering the field dependence of  $\lambda_N$  and  $1/\tau_s$ , we have shown that this strong field dependence originates from Kondo scattering in the NM channel, and that application of an external magnetic field quenches this scattering. We have successfully applied a model for Kondo scattering in a magnetic field to describe the spin-flip scattering rate data, demonstrating quantitative agreement with experiment and providing the first measurements of the field dependence of the Kondo EY parameter,  $\beta_K(H)$ . This work thus resolves the long-standing mystery of the origin of this high field dependence, and points to a systematic underestimation of  $\tau_s$  in NLSVs where MIs are present. Due to the low value of  $\beta_K \sim 3/2$ , this effect is significant, and is likely to be measurable in a variety of all-metallic NLSVs. By application of a magnetic field, however, we have demonstrated a simple means to remove the suppression and restore the non-local resistance to its Kondo-free value, obviating the need for additional material considerations or the inclusion of a diffusion-limiting interlayer.

## ACKNOWLEDGEMENTS

Work supported by the UK EPSRC, Grant No. EP/P005713/1, and the National Science Foundation under Award Number DMR-1807124. Parts of this work were performed in the Characterization Facility, UMN, which receives partial support from NSF through the MSREC program. Other parts of this work were conducted in the Minnesota Nano Center, which is

1 supported by the NSF through the National Nano Coordinated Infrastructure Network, under  
2 Award Numbers NNCI-1542202 and ECCS-2025124.

3



## REFERENCES

- <sup>1</sup> M. Yamada, D. Sato, N. Yoshida, M. Sato, K. Meguro, and S. Ogawa, *IEEE Trans. Magn.* **49**, 713 (2013).
- <sup>2</sup> Y.K. Takahashi, S. Kasai, S. Hirayama, S. Mitani, and K. Hono, *Appl. Phys. Lett.* **100**, 052405 (2012).
- <sup>3</sup> M. Takagishi, K. Yamada, H. Iwasaki, H.N. Fuke, and S. Hashimoto, *IEEE Trans. Magn.* **46**, 2086 (2010).
- <sup>4</sup> M. Johnson and R.H. Silsbee, *Phys. Rev. Lett.* **55**, 1790 (1985).
- <sup>5</sup> F.J. Jedema, A.T. Filip, and B.J. van Wees, *Nature* **410**, 345 (2001).
- <sup>6</sup> G. Mihajlović, S.I. Erlingsson, K. Výborný, J.E. Pearson, S.D. Bader, and A. Hoffmann, *Phys. Rev. B* **84**, 132407 (2011).
- <sup>7</sup> H. Idzuchi, Y. Fukuma, L. Wang, and Y. Otani, *Appl. Phys. Lett.* **101**, 022415 (2012).
- <sup>8</sup> H. Zou and Y. Ji, *Appl. Phys. Lett.* **101**, 082401 (2012).
- <sup>9</sup> S. Rakheja, S.C. Chang, and A. Naeemi, *IEEE Trans. Electron Devices* **60**, 3913 (2013).
- <sup>10</sup> E. Villamor, M. Isasa, L.E. Hueso, and F. Casanova, *Phys. Rev. B* **88**, 184411 (2013).
- <sup>11</sup> E. Villamor, M. Isasa, L.E. Hueso, and F. Casanova, *Phys. Rev. B* **87**, 094417 (2013).
- <sup>12</sup> S. Chen, H. Zou, C. Qin, and Y. Ji, *Appl. Phys. Express* **7**, 113001 (2014).
- <sup>13</sup> J.T. Batley, M.C. Rosamond, M. Ali, E.H. Linfield, G. Burnell, and B.J. Hickey, *Phys. Rev. B* **92**, 220420 (2015).
- <sup>14</sup> Y. Cai, Y. Luo, C. Zhou, C. Qin, S. Chen, Y. Wu, and Y. Ji, *J. Phys. D: Appl. Phys.* **49**, 185003 (2016).
- <sup>15</sup> F.J. Jedema, M.S. Nijboer, A.T. Filip, and B.J. van Wees, *Phys. Rev. B* **67**, 085319 (2003).

- <sup>16</sup> S.O. Valenzuela and M. Tinkham, *Appl. Phys. Lett.* **85**, 5914 (2004).
- <sup>17</sup> Y. Ji, A. Hoffmann, J.S. Jiang, and S.D. Bader, *Appl. Phys. Lett.* **85**, 6218 (2004).
- <sup>18</sup> S. Garzon, I. Žutić, and R.A. Webb, *Phys. Rev. Lett.* **94**, 176601 (2005).
- <sup>19</sup> T. Kimura, T. Sato, and Y. Otani, *Phys. Rev. Lett.* **100**, 066602 (2008).
- <sup>20</sup> X.J. Wang, H. Zou, and Y. Ji, *Phys. Rev. B - Condens. Matter Mater. Phys.* **81**, 1 (2010).
- <sup>21</sup> G. Mihajlović, J.E. Pearson, S.D. Bader, and A. Hoffmann, *Phys. Rev. Lett.* **104**, 237202 (2010).
- <sup>22</sup> M. Erekhinsky, A. Sharoni, F. Casanova, and I.K. Schuller, *Appl. Phys. Lett.* **96**, 022513 (2010).
- <sup>23</sup> N. Poli, M. Urech, V. Korenivski, and D.B. Haviland, *J. Appl. Phys.* **99**, 2004 (2006).
- <sup>24</sup> A. Fert and P.M. Levy, *Phys. Rev. Lett.* **106**, 157208 (2011).
- <sup>25</sup> Y. Otani and T. Kimura, *Philos. Trans. R. Soc. A Math. Phys. Eng. Sci.* **369**, 3136 (2011).
- <sup>26</sup> K. Výborný, G. Mihajlović, A. Hoffmann, and S.I. Erlingsson, *J. Phys. Condens. Matter* **25**, 216007 (2013).
- <sup>27</sup> K.S. Das, F.K. Dejene, B.J. van Wees, and I.J. Vera-Marun, *Phys. Rev. B* **94**, 180403 (2016).
- <sup>28</sup> D. Ruffer, F.D. Czeschka, R. Gross, and S.T.B. Goennenwein, *Appl. Phys. Lett.* **99**, (2011).
- <sup>29</sup> Y. Niimi, D. Wei, H. Idzuchi, T. Wakamura, T. Kato, and Y. Otani, *Phys. Rev. Lett.* **110**, 016805 (2013).
- <sup>30</sup> C. Zhou, F. Kandaz, Y. Cai, C. Qin, M. Jia, Z. Yuan, Y. Wu, and Y. Ji, *Phys. Rev. B* **96**, 094413 (2017).

- <sup>31</sup> P.K. Muduli, M. Kimata, Y. Omori, T. Wakamura, S.P. Dash, and Y. Otani, *Phys. Rev. B* **98**, 024416 (2018).
- <sup>32</sup> M. Johnson and R.H. Silsbee, *Phys. Rev. B* **76**, 153107 (2007).
- <sup>33</sup> F.L. Bakker, A. Slachter, J.P. Adam, and B.J. Van Wees, *Phys. Rev. Lett.* **105**, 1 (2010).
- <sup>34</sup> M. Erekhinsky, F. Casanova, I.K. Schuller, and A. Sharoni, *Appl. Phys. Lett.* **100**, 212401 (2012).
- <sup>35</sup> A. Hojem, D. Wesenberg, and B.L. Zink, *Phys. Rev. B* **94**, 1 (2016).
- <sup>36</sup> F. Casanova, A. Sharoni, M. Erekhinsky, and I.K. Schuller, *Phys. Rev. B* **79**, 1 (2009).
- <sup>37</sup> S. Takahashi and S. Maekawa, *Phys. Rev. B - Condens. Matter Mater. Phys.* **67**, 1 (2003).
- <sup>38</sup> R.J. Elliott, *Phys. Rev.* **96**, 266 (1954).
- <sup>39</sup> Y. Yafet, in *Solid State Phys.* (Academic Press, 1963), pp. 1–98.
- <sup>40</sup> P. Monod and F. Beuneu, *Phys. Rev. B* **19**, 911 (1979).
- <sup>41</sup> J.D. Watts, L. O’Brien, J.S. Jeong, K.A. Mkhoyan, P.A. Crowell, and C. Leighton, *Phys. Rev. Mater.* **3**, 124409 (2019).
- <sup>42</sup> L. O’Brien, D. Spivak, J.S. Jeong, K.A. Mkhoyan, P.A. Crowell, and C. Leighton, *Phys. Rev. B* **93**, 014413 (2016).
- <sup>43</sup> J.D. Watts, J.S. Jeong, L. O’Brien, K.A. Mkhoyan, P.A. Crowell, and C. Leighton, *Appl. Phys. Lett.* **110**, 222407 (2017).
- <sup>44</sup> K.W. Kim, L. O’Brien, P.A. Crowell, C. Leighton, and M.D. Stiles, *Phys. Rev. B* **95**, 1 (2017).
- <sup>45</sup> K. Hamaya, T. Kurokawa, S. Oki, S. Yamada, T. Kanashima, and T. Taniyama, *Phys. Rev. B* **94**, 140401 (2016).

- <sup>46</sup> L. O'Brien, M.J. Erickson, D. Spivak, H. Ambaye, R.J. Goyette, V. Lauter, P.A. Crowell, and C. Leighton, *Nat. Commun.* **5**, 3927 (2014).
- <sup>47</sup> J.A. Mydosh, *Spin Glasses: An Experimental Introduction* (Taylor & Francis, London, 1993).
- <sup>48</sup> G. Gruner and A. Zawadowski, *Reports Prog. Phys.* **37**, 1497 (1974).
- <sup>49</sup> J. Kondo, S. Koikegami, K. Odagiri, K. Yamaji, and T. Yanagisawa, *The Physics of Dilute Magnetic Alloys* (Cambridge University Press, Cambridge, 2012).
- <sup>50</sup> S.P. Dash, S. Sharma, J.C. Le Breton, J. Peiro, H. Jaffrès, J.-M. George, A.L. Lemaître, and R. Jansen, *Phys. Rev. B* **84**, 54410 (2011).
- <sup>51</sup> K.M. McCreary, A.G. Swartz, W. Han, J. Fabian, and R.K. Kawakami, *Phys. Rev. Lett.* **109**, 186604 (2012).
- <sup>52</sup> S. Vélez, V.N. Golovach, A. Bedoya-Pinto, M. Isasa, E. Sagasta, M. Abadia, C. Rogero, L.E. Hueso, F.S. Bergeret, and F. Casanova, *Phys. Rev. Lett.* **116**, 016603 (2016).
- <sup>53</sup> R.K. Bennet, A. Hojem, and B.L. Zink, *Phys. Rev. B* **100**, 104404 (2019).
- <sup>54</sup> See Supplemental Material at [URL] for further discussion on  $\delta R_{NL}$  and  $R_b$  in other material pairings and the isotropy of  $\delta R_{NL}$  with field direction.
- <sup>55</sup> See Supplemental Material at [URL] for further discussion on Brillouin fits and Langevin fits to  $\delta R_{NL}/R_{spin}$ .
- <sup>56</sup> S. Takahashi and S. Maekawa, *Phys. C Supercond. Its Appl.* **437–438**, 309 (2006).
- <sup>57</sup> J. Bass and W.P. Pratt, *J. Phys. Condens. Matter* **19**, (2007).
- <sup>58</sup> F. Beuneu and P. Monod, *Phys. Rev. B* **18**, 2422 (1978).
- <sup>59</sup> K. Inoue and Y. Nakamura, *Phys. Status Solidi* **58**, 355 (1973).

- <sup>60</sup> D. Goldhaber-Gordon, J. Göres, M.A. Kastner, H. Shtrikman, D. Mahalu, and U. Meirav, *Phys. Rev. Lett.* **81**, 5225 (1998).
- <sup>61</sup> W. Wei and G. Bergmann, *Phys. Rev. B* **37**, 5990 (1988).
- <sup>62</sup> P. Monod, *Phys. Rev. Lett.* **19**, 1113 (1967).
- <sup>63</sup> E.W. Fenton, *Phys. Rev. B* **7**, 3144 (1973).
- <sup>64</sup> V.I. Litvinov, *Phys. Status Solidi* **77**, 71 (1976).
- <sup>65</sup> A.A. Abrikosov, *Phys. Phys. Fiz.* **2**, 61 (1965).
- <sup>66</sup> H. Rohrer, *Phys. Rev.* **174**, 583 (1968).
- <sup>67</sup> See Supplemental Material at [URL] for further discussion on fitting the spin relaxation rate with an alternative Kondo model.
- <sup>68</sup> J. Kondo, *Prog. Theor. Phys.* **32**, 37 (1964).
- <sup>69</sup> J.A. Appelbaum, *Phys. Rev.* **154**, 633 (1967).
- <sup>70</sup> E.L. Wolf and D.L. Losee, *Phys. Rev. B* **2**, 3660 (1970).
- <sup>71</sup> J. Fabian, A. Matos-Abiague, C. Ertler, P. Stano, and I. Zutic, *Acta Phys. Slovaca* **57**, 565 (2007).
- <sup>72</sup> Y.J. Uemura, T. Yamazaki, D.R. Harshman, M. Senba, and E.J. Ansaldo, *Phys. Rev. B* **31**, 546 (1985).
- <sup>73</sup> M.B. Salamon, *Phys. Rev.* **155**, 224 (1967).
- <sup>74</sup> Y. Niimi, M. Kimata, Y. Omori, B. Gu, T. Ziman, S. Maekawa, A. Fert, and Y. Otani, *Phys. Rev. Lett.* **115**, 196602 (2015).
- <sup>75</sup> T. Uchiyama, M. Matsui, and K. Adachi, *IEEE Trans. Magn.* **23**, 2305 (1987).
- <sup>76</sup> D. Korn and G. Zibold, *J. Phys. F Met. Phys.* **15**, 2497 (1985).

<sup>77</sup> M.-K. Hou, M.B. Salamon, and T.A.L. Ziman, Phys. Rev. B **30**, 5239 (1984).

## Figures

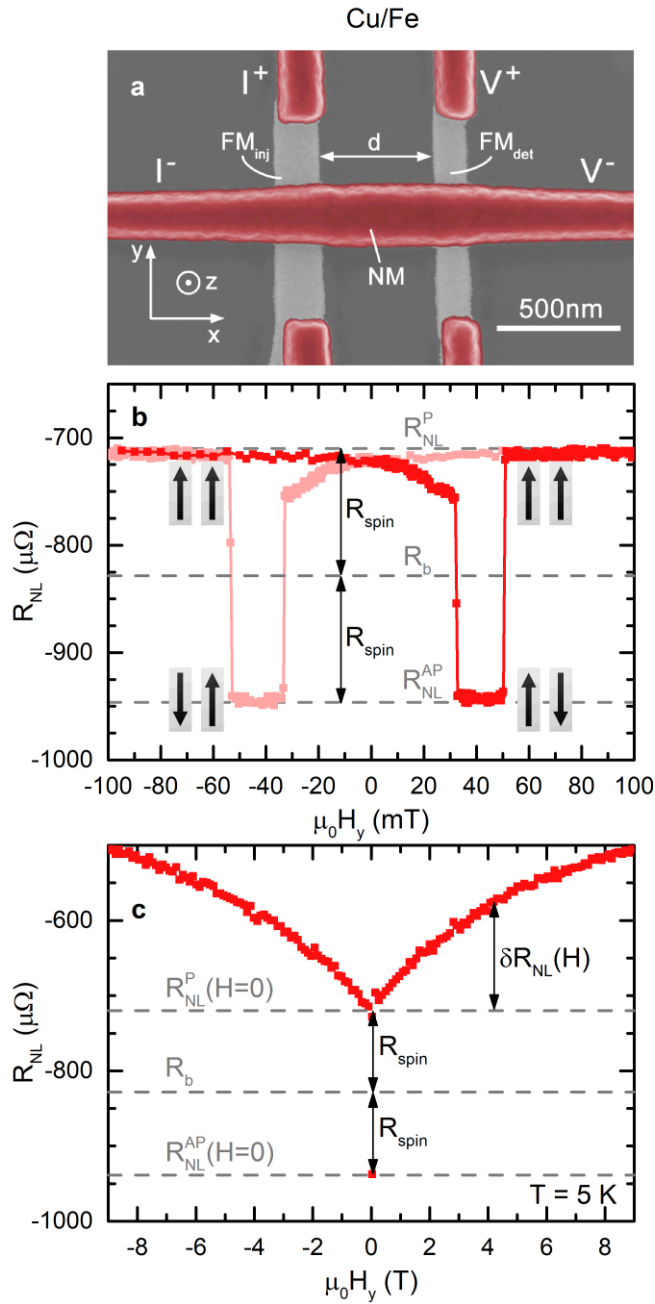


**Figure 1** (a) False color SEM image of a Cu/Fe NLSV, with the non-magnetic metal (NM) and ferromagnetic (FM) materials highlighted. In the non-local geometry, a current ( $I$ ) is injected at  $FM_{inj}$  and extracted from the far-left side of the NM channel, resulting in a non-equilibrium spin accumulation, manifest as a voltage ( $V_{NL}$ ), measured between the far right of the NM channel and  $FM_{det}$ . (b) In-plane magnetic field ( $H_y$ ) dependence of the non-local resistance,  $R_{NL} = V_{NL}/I$ , for a Cu/Fe NLSV with  $d = 750$  nm, for forward (red) and reverse (pink) sweeps. The magnetization direction of the FM contacts are indicated by the arrows.  $R_b = (R_{NL}^P + R_{NL}^{AP})/2$  is indicated on the figure. (c) Same as (b) up to larger (9 T) magnetic fields. Red solid squares show the measured data for parallel alignment of the FM contacts. The anti-parallel response at zero field is also shown, and the definitions of  $R_{spin}$  and  $\delta R_{NL}$

are indicated.  $R_{NL}^P$  increases with field strength, beginning to saturate at sufficiently high fields, indicating a suppression of spin-flip scattering.



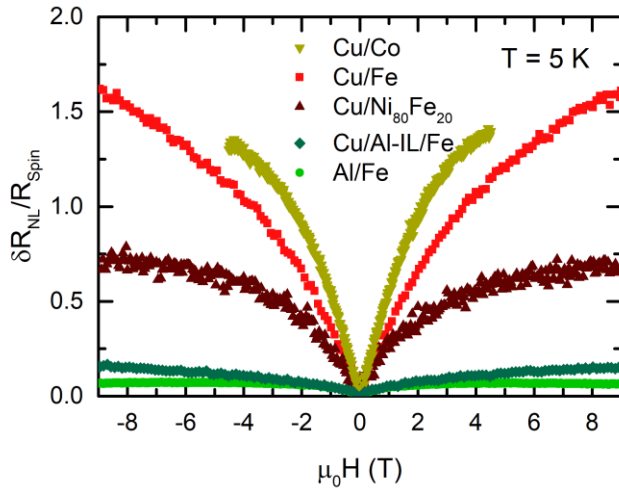


**Figure 2** (Normalized)  $\delta R_{NL}/R_{Spin}$  as a function of in-plane applied magnetic field, for various materials. Devices shown have  $d = 500$  nm except for Cu/Co and Cu/Ni<sub>80</sub>Fe<sub>20</sub> which have  $d = 400$  nm. Measurements of Cu/Co were taken only up to an applied field of  $\mu_0 H = \pm 4.5$  T. The effect of in-plane applied magnetic field is most prominent for Cu/Co and Cu/Fe. For Cu/Al IL/Fe and Al/Fe, the effect is almost negligible.

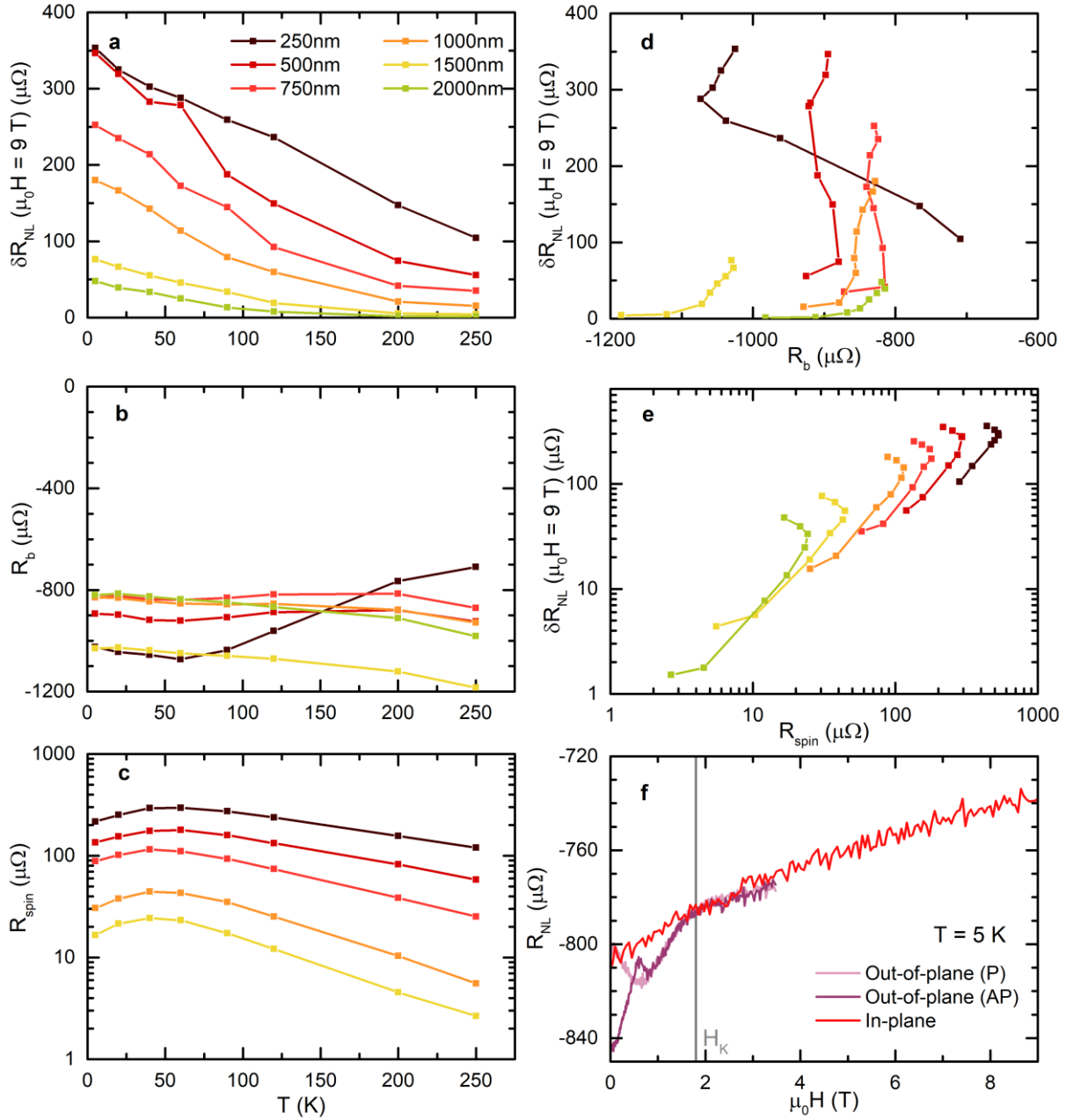


**Figure 3** Temperature evolution of **(a)**  $\Delta R_{NL}(\mu_0 H = 9 T)$ , **(b)**  $R_b$  and **(c)**  $R_{spin}$  for Cu/Fe NLSVs of various  $d$ . **(d)** Direct comparison of  $\Delta R_{NL}(\mu_0 H = 9 T)$  and  $R_b$ , demonstrating no correlation between the two parameters, and hence ruling out background effects as the origin of  $\Delta R_{NL}$ . **(e)**  $\Delta R_{NL}(\mu_0 H = 9 T)$  as a function of  $R_{spin}$ . A clear, consistent correlation exists between the two, highlighting that  $\Delta R_{NL}$  arises from spin-transport-related effects. **(f)** Field enhancement of  $R_{NL}$  for in-plane and out-of-plane (Hanle) measurements for a  $d = 2000$  nm Cu/Fe NLSV at 5 K. Beyond the saturation field ( $H_K$ ) of the FM contacts (vertical grey line) the in-plane and out-of-plane field responses of  $R_{NL}$  are identical, indicating that  $\Delta R_{NL}$  is independent of applied field direction.

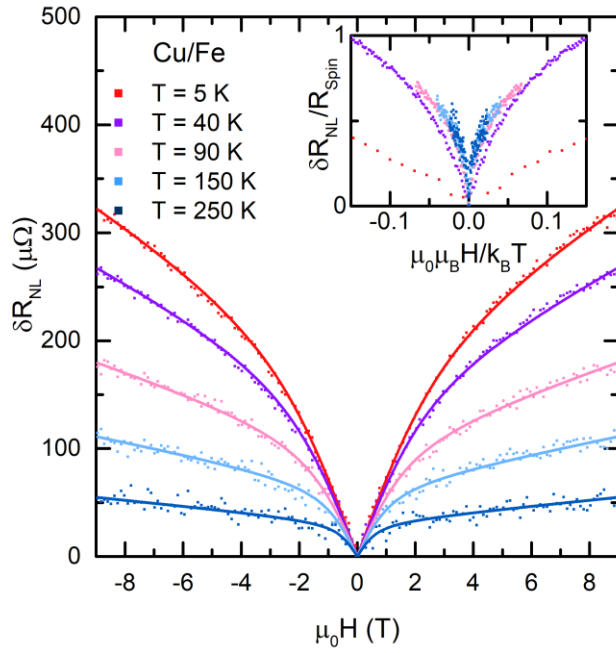


**Figure 4**  $\delta R_{NL}$  as a function of  $\mu_0 H$  for a Cu/Fe NLSV with  $d = 500$  nm, at various temperatures. Solid lines are fits using equation (3), in order to model the data as a continuous function of field. Inset shows  $\delta R_{NL}$  normalized to  $R_{spin}$  as a function of  $\mu_0 \mu_B H / k_B T$  for the same device. The 5 K data extends beyond the range of the plot. The data clearly do not collapse onto a single form, indicating that the field enhancement is not simply due to alignment of magnetic impurities.

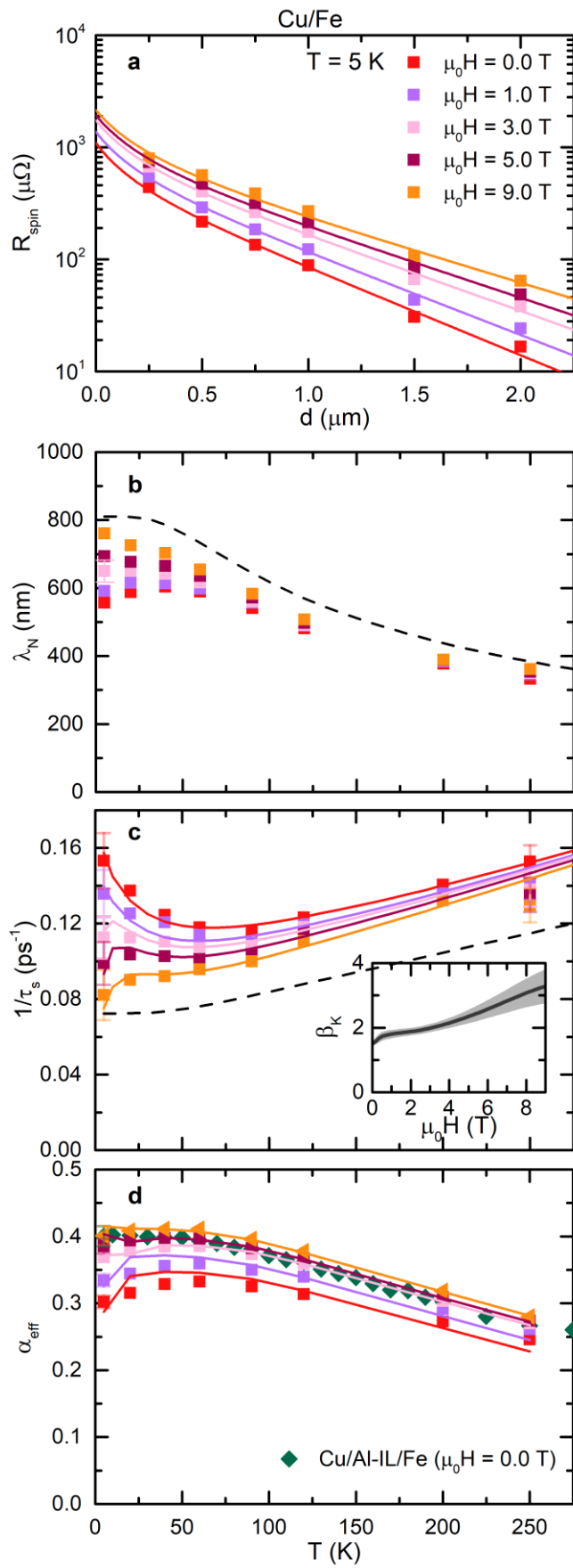


**Figure 5** Data from measurements of Cu/Fe devices. For clarity, only select field strengths are shown, although a continuous range was available to us. **(a)** Variation of  $R_{spin}(H)$  with  $d$ . Error bars are smaller than the symbol size. Solid lines are fits to the data using equation (4). **(b)** Spin diffusion length ( $\lambda_N$ ) in the NM channel as a function of temperature. The dashed line is an estimate of the spin diffusion length from phonon and impurity scattering only. Error bars are smaller than the symbol size. **(c)** Same as (b) but for spin-flip scattering rate ( $1/\tau_s$ ). Solid lines are fits using equations (1) and (6). For clarity, error bars are only shown for the first data points and last data points. (Inset) Quasi-continuous variation of  $\beta_K$  with field strength from fitting of data in (c). The light grey shaded area represents the uncertainty in the fit values. **(d)** Effective spin polarization,  $\alpha_{eff}$  as a function of temperature. The zero-field and high-field (9 T) data are shown for a Cu/Fe device. Data from a Cu/Al-IL/Fe device at zero-field are also shown for comparison. Both devices have  $d = 500$  nm. Under a high-field,  $\alpha_{eff}$  for the Cu/Fe closely follows that of the Cu/Al-IL/Fe device, indicating that “normal” behavior has been restored.

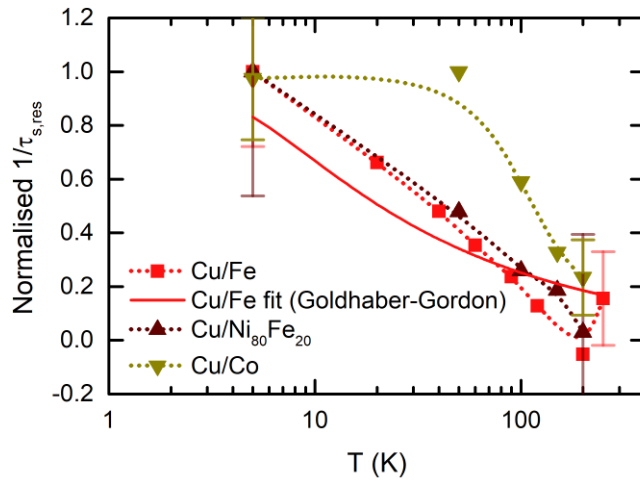


**Figure 6** Normalized residual spin relaxation rate ( $1/\tau_{s,res} = 1/\tau_s^{low\ field} - 1/\tau_s^{high\ field}$ ) as a function of temperature ( $\log_{10}$  scale), for Cu/Co, Cu/Fe and Cu/Ni<sub>80</sub>Fe<sub>20</sub>. The Cu/Fe data are fit using the phenomenological Goldhaber-Gordon expression of equation (5) (solid, red line). The Cu/Co and Cu/Ni<sub>80</sub>Fe<sub>20</sub> data sets are incomplete and so should be treated only qualitatively. For these data, a guide to the eye (dotted line) is given. For clarity, error bars for only the first and last data points are shown.

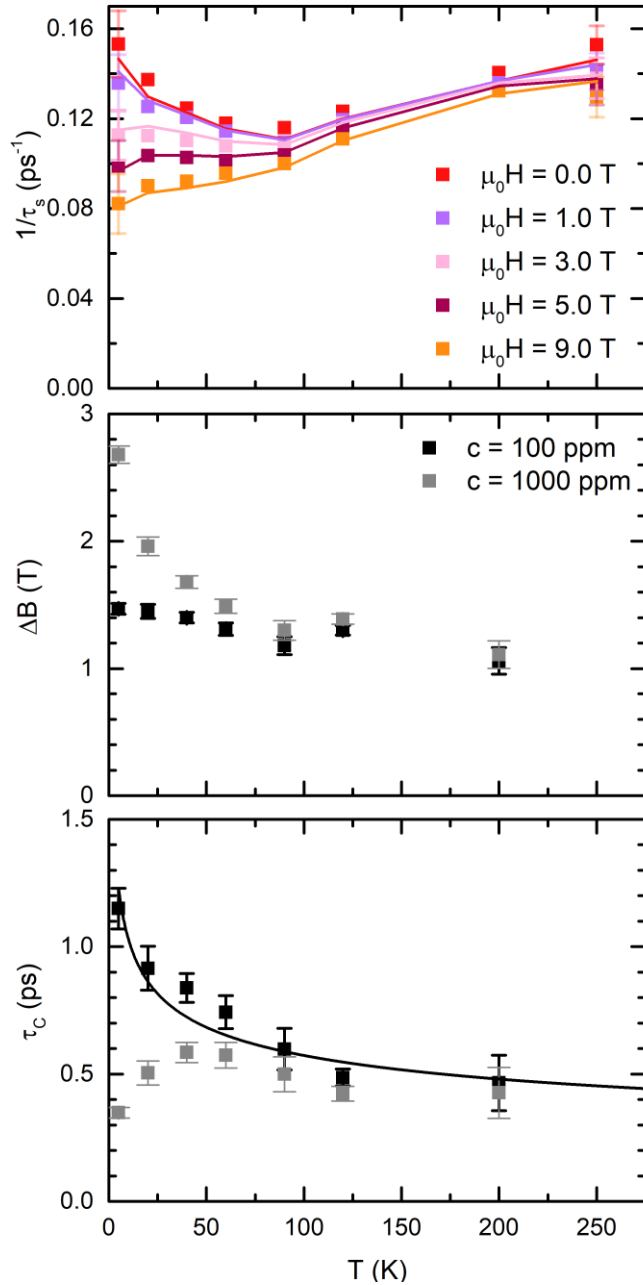


**Figure 7 (a)** The  $1/\tau_s$  data (squares) for Cu/Fe NLSVs fit using equation (8) (solid lines), in order to test the applicability of the exchange model. The data are the same as in Fig. 5(c). A reasonable agreement between the data and the fit is achieved. Parameters **(b)**  $\Delta B$  and **(c)**  $\tau_c$  extracted from the fitting in (a) for  $c = 100$  ppm and 1000 ppm, shown as a function of temperature. For  $c = 100$  ppm,  $\Delta B$  is independent of temperature, whereas  $\tau_c$  increases with decreasing temperature, possibly indicating a spin glass transition. Fitting using a conventional description for spin glass dynamics (equation (10); solid line) reveals an unreasonably slow transition rate, however, indicating that a spin glass transition does not suitably describe the system.  $c = 1000$  ppm yields an unreasonably large  $\Delta B$  and non-trivial  $T$  dependence of  $\tau_c$ . Anomalous 250 K data in  $\Delta B$  and  $\tau_c$  (likely arising from the large spread in  $1/\tau_s$ ) have been removed.